www.czasopisma.pan.pl PAN POLSKA AKADEMIA NAUK www.journals.pan.pl

Arch. Metall. Mater. **66** (2021), 1, 81-89

DOI: 10.24425/amm.2021.134762

M. MIČIAN[1*], J. WINCZEK[2], D. HARMANIAK[1], R. KOŇÁR[1], M. GUCWA[2], J. MORAVEC[3]

PHYSICAL SIMULATION OF INDIVIDUAL HEAT-AFFECTED ZONES IN S960MC STEEL

This research is focused on the analysis of heat-affected sub-zones in 2 mm thick steel S960MC samples, with the aim of observing and evaluating the mechanical properties after exposure to temperatures corresponding to individual heat-affected sub-zones. Test samples were prepared using a Gleeble 3500 thermo-mechanical simulator. The samples were heated in the range from 550°C to 1350°C and were subsequently quickly cooled. The specimens, together with the base material, were then subjected to tensile testing, impact testing, and micro-hardness measurements in the sample cross-section, as well as evaluation of their microstructure. Fracture surfaces are investigated in samples after impact testing. The heat-affected sub-zones studied indicate high sensitivity to the thermal input of welding. There is a significant decrease in tensile strength and yield strength at temperatures around 550°C.

Keywords: mechanical properties of heat affected zone, steel S960MC, physical simulation, Gleeble 3500

1. Introduction

High-strength steels are in great demand, due to their excellent mechanical properties. They offer high strength, as well as sufficient toughness and formability. Their main use is in the production of lifting equipment, mobile cranes, or in the manufacture of axle and chassis parts. The weight of the entire device can be reduced, thanks to the high strength of the steel, which translates into reduced fuel consumption and CO_2 emissions [1-4]. As the favourable mechanical properties of high-strength steel is achieved by thermal-mechanical processing, heat input to the material during the welding process can significantly affect the resulting microstructure, thereby influencing the properties of the welded joint. The main role of modern welding engineers is to establish welding methods and procedures that least affect the base material near the weld, in order to keep the mechanical properties of the heat-affected zone (HAZ) similar to those of the base material, thus exploiting the high potential of HSLA steels. One of the problems which can occur during the welding of these steels is the formation of a "soft zone" in the HAZ, in which the strength and hardness of the material are reduced [1,5-9].

Several experiments have shown that the best welding results for these steels occur with low heat input, as a reduced heat input leads to narrowing of the soft zone [7]. A narrower soft zone improves the final properties of the weld. Therefore, several studies have focused on the use of welding methods with a concentrated heat source, such as a laser or electron beam [10-12]. The heat input is related to the weld cooling time and the $t_{8/5}$ parameter, which represents the cooling time in the HAZ between 800°C and 500°C; the interval in which the most important structural changes occur in the steel. The width of the soft zone increases with increasing $t_{8/5}$ time. Previous experiments have confirmed that, as the $t_{8/5}$ time increases, the yield strength and tensile strength decrease; while the impact strength value may increase, in some cases [13]. Experiments utilising an additional cooling device during welding, leading to a shorter $t_{8/5}$ time, have been shown to manifest a smaller decrease in strength [14,15].

As the microstructure determines the steel mechanical properties, it is important to minimize the negative effects of the thermal cycle on the microstructure. In a HAZ, the grain size increases due to increasing heat, which – together with carbides and other structural changes -– leads to deterioration of the weld mechanical properties. Every HAZ can be divided into several sub-zones: in the case of single-layer welds, these are the coarse-grained HAZ (CGHAZ), fine-grained HAZ (FGHAZ), intercritical HAZ (or partially transformed zone; ICHAZ), and the sub-critical HAZ (or annealed zone; SCHAZ) [16-18]. However, the typical size of a sub-zone is too small and unsuitable for some types of tests, especially mechanical tests. With a thermo-mechanical simulator, such as the Gleeble 3500 used

[1] UNIVERSITY OF ŽILINA, FACULTY OF MECHANICAL ENGINEERING, 8215/1 UNIVERZITNÁ STR., 010 26 ŽILINA, SLOVAK REPUBLIC
[2] CZESTOCHOWA UNIVERSITY OF TECHNOLOGY, FACULTY OF MECHANICAL ENGINEERING AND COMPUTER SCIENCE, 69 DABROWSKIEGO STR., 42-201 CZESTOCHOWA, POLAND
[3] TECHNICAL UNIVERSITY OF LIBEREC, FACULTY OF MECHANICAL ENGINEERING, 1402/2 STUDENTSKÁ STR., 461 17 LIBEREC I, CZECH REPUBLIC

* Corresponding author: milos.mician@fstroj.uniza.sk

in our experiments, it is possible to create the required part of the HAZ in sufficient volume for further experiments and, at the same time, ensure high reproducibility of the samples [19-21].

2. Materials and methods

Experimental S960MC Material

The chemical composition of the investigated S960MC base material, according to the material certificate, is summarized in Table 1. Table 2 summarizes the mechanical properties of the examined S960MC steel, as required, from the inspection certificate and our own measurements. The examined steel has a guaranteed 27J Charpy-V energy (CVN) at −40°C (for standard sample width of 10 mm). Our CVN measurement was performed with a reduced material thickness of t = 2 mm. To compare the results of 2 mm wide samples with the criterion value, the results were recalculated using the coefficient given by the ratio of standard width and reduced width (i.e., 10 mm / 2 mm = 5). The same approach was also used in the works of Schneider et al. [1] and Guo [22].

The studied steel microstructure comprised a mixture of martensite and tempered martensite. This kind of structure allows for a combination of very good mechanical properties and high toughness.

Preparation of Test Samples and Their Physical Simulation on Gleeble

Physical simulations provide unique opportunities for HAZ characterization in metals during different kinds of fusion welding techniques. Individual HAZ regions depend on their different thermal history. Experimental simulations of arc welding thermal cycles were carried out using a Gleeble 3500 thermal-mechanical simulator. Using HAZ testing, the desired part of the HAZ can be precisely and homogeneously created in a volume sufficient for further material tests (e.g., for the Charpy V-notch pendulum impact test or tensile test). The samples tested using the Gleeble device were laser cut from sheet metal of thickness t = 3 mm and then ground to a thickness of 2 mm such that they could be clamped into the jaws of the Gleeble device [13]. The overall dimensions of the test sample for the Gleeble simulation are shown in Fig. 1. A thermocouple Welder (type 35200) was used to attach individual thermocouple K-type wires to the Gleeble specimens. Thermocouple wires were welded to the centre of the sample (see Fig. 2).

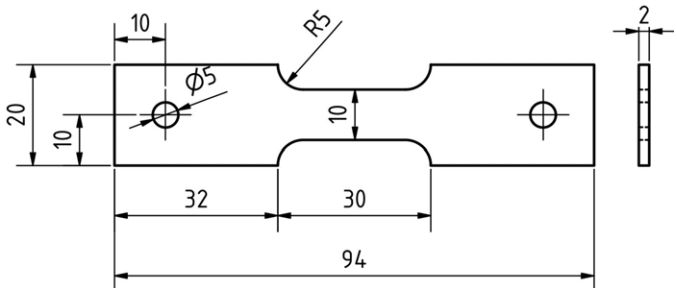

Fig. 1. Dimensions of the samples for testing on a Gleeble 3500 device (unit: mm)

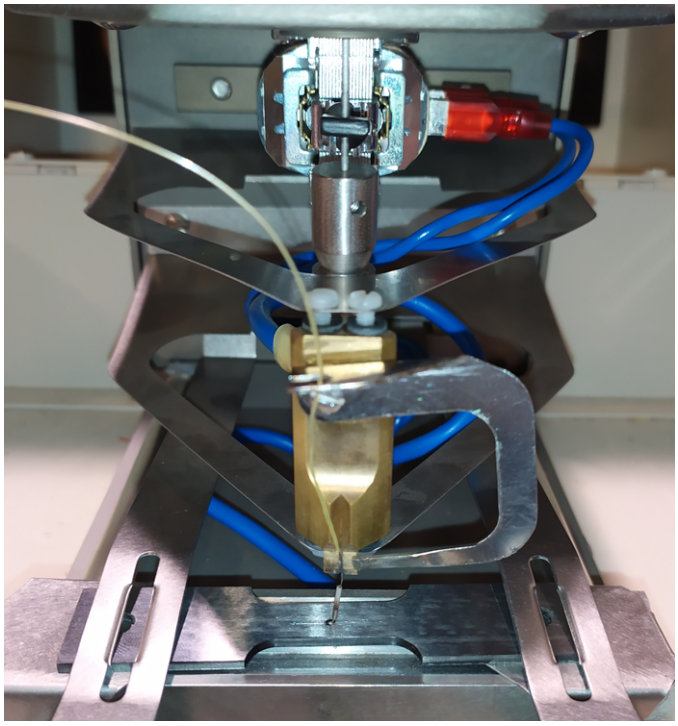

Fig. 2. Preparation of the sample by welding a thermocouple

TABLE 1

Chemical composition of the investigated S960MC steel

Chemical composition (wt.%)											
C	Si	Mn	P	S	Al	Nb	V	Ti	Cr	Ni	Mo
0.09	0.18	1.06	0.01	0.003	0.036	0.002	0.007	0.03	1.08	0.07	0.11

TABLE 2

Mechanical properties of the investigated S960MC steel

According to	$R_{p0.2}$ [MPa]	R_m [MPa]	$R_{p0.2}$ / R_m	A [%]	KV[J]
EN 10149-2	min. 960	980-1250	—	min. 7	min. 27 J / –40°C
Inspection Certificate	1018	1108	0.92	10	—
Experimental measurements	1007	1092	0.92	7.9	85 J / –40°C

This thermocouple sensed the real temperature during heating and cooling. At the same time, the cycle was compared with the program cycle, and the control system adjusted the power to achieve matching of the two cycles. The Gleeble control program defined the sample heating rate conditions, the hold time at the target temperature, and the frequency of reading the values. The heating rate was based on the real temperature cycle measured during welding in a previous experiment [13]. This heating rate was at a level of 320°C/s. Individual samples were heated to 1350°C, 1200°C, 1000°C, 800°C, 650°C, 600°C, and 550°C. The residence time at maximum temperature was 0.5 s. The samples were then cooled freely, without further reheating. Seven samples were simulated for each maximum cycle temperature, for a total of 49 samples. The test samples were labelled according to their maximum cycle temperature (e.g., T1350, T1200, T1000, and so on). The temperature cycles measured for one sample at its respective maximum temperature are shown in Fig. 3.

For temperature cycles whose maximum peak exceeded a temperature of 800°C, it was possible to determine the cooling time $t_{8/5}$: At temperature cycle T800, $t_{8/5}$ was equal to 15.8 s; at T1000 $t_{8/5}$ was equal to 19.1 s; at T1200, $t_{8/5}$ was equal to 25.8 s; and, at T1350, $t_{8/5}$ was equal to 26.5 s. The whole process took place in vacuum. Samples coming directly from the Gleeble device were used for static tensile testing without further treatment or modification. The test was performed on an INSTRON Model 5985 device at room temperature. Fig. 4 shows a diagram of a sample with required dimensions for a Charpy pendulum impact test with maximum impact energy of 150 J.

The Charpy pendulum impact test was performed on four samples from each temperature cycle. The test was performed on 2 × 10 × 55 mm samples at –40°C. Samples of the same width were also made from the base material (BM). The criterion value of absorbed energy for S960MC steel at –40°C is KV = 27 J in the case of samples with a standard 10 mm width. To compare

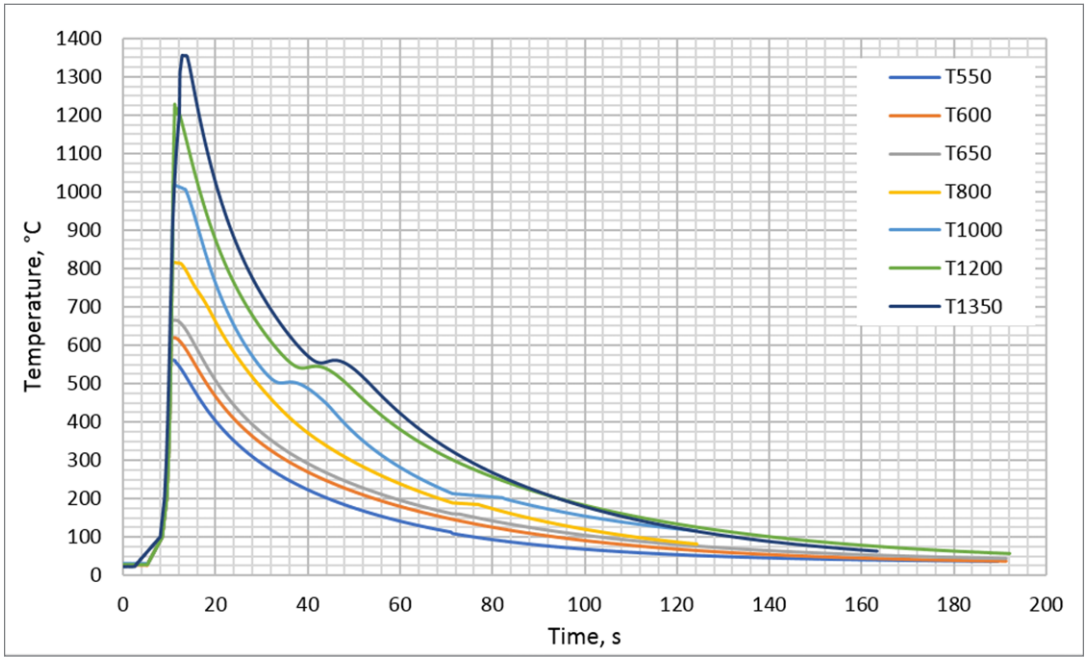

Fig. 3. Thermal cycle from GLEEBLE physical simulations

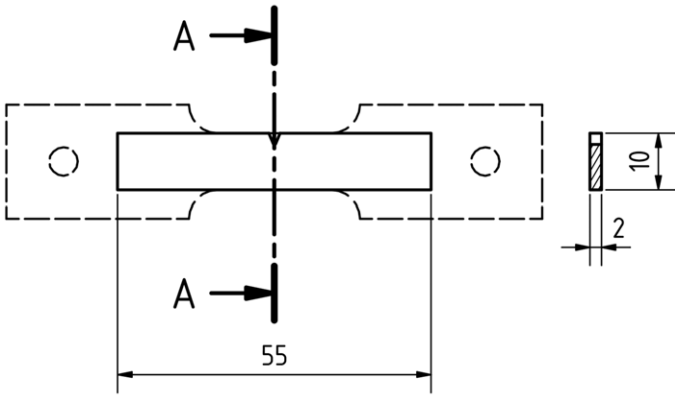

Fig. 4. Sample with reduced 2-mm thickness used to measure the Charpy pendulum impact test (unit: mm)

the results of 2 mm wide samples with the criterion value, the results were recalculated. Fracture surfaces after the impact test were imaged by an SEM microscope, model TESLA VEGA II. Samples for the assessment of microstructure and microhardness were taken by means of a longitudinal section using precise water-cooled cutting equipment, in order to avoid any heat effect on the samples. The above-mentioned samples were prepared using a standard procedure for light metallographic microscopy and etched with 2% Nital. The samples were assessed using a ZEISS LSM 700 optical microscope. Their microhardness was measured in the centre of the sample using an Innovatest NOVA 130 device; this measuring device utilized a load force of 9.807 N for 10 s. Hardness was measured in three lines, where three indents were made in each line. The distance between the lines and the indents in the line was 0.5 mm.

3. Results and discussion

Tensile test

Tensile tests were performed according to the EN ISO 6892-1 standard. Two samples were used for each maximum cycle temperature. Table 3 shows the average values of yield strength, tensile strength, and the ratio of yield strength to tensile strength. The tensile test results are presented in Table 3 and graphically shown in Fig. 5.

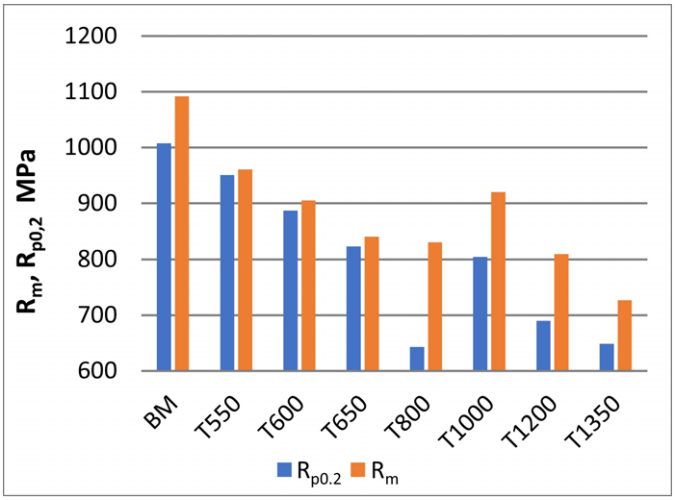

Fig. 5. Yield strength and tensile strength of the base material and samples with different maximal temperature

Reference values of yield strength and tensile strength were given by the mechanical properties of the base material without thermal loading. All samples that had been loaded with various temperature cycles showed a significant decrease in their yield strength and tensile strength. In the range of maximum temperatures reaching 550-650°C, there was an almost linear decrease in the yield strength and tensile strength, compared to the base material (i.e., a higher maximum temperature means a larger decrease). This was related to the effect of tempering the martensitic structure of the base material before reaching the A_{c1} transformation temperature. The samples showed the lowest yield strength decrease when heated to the maximum cycle temperature of 800°C. The decrease was 64% yield strength value, compared to the base material. The reason for the above-mentioned decrease was heating up to temperatures ranging from Ac_1 to Ac_3, where martensite was partially transformed into austenite. This temperature exposure resulted in the formation of a mixture of martensite and austenite, which transformed into martensite (due to the slower cooling) and ferrite, while the untransformed martensite was tempered. The ferrite-containing structures achieved the lowest yield strength vs. yield strength ratio compared to other samples. The sample affected by the temperature cycle with a maximum temperature of 1000°C re-increased yield strength and tensile strength, which meant heating slightly above the Ac_3 temperature. This caused the transformation of the base martensitic microstructure to austenite. However, due to the relatively low temperature (compared with CGHAZ) and rapid cooling, it resulted in a refinement of the austenitic microstructure and, later, of the resulting martensitic fine-grain microstructure as well. Higher temperatures resulted in a drop in both the yield strength and tensile strength. When heating the samples using a temperature cycle with the maximum value of 1350 °C, the strength was the lowest, reaching only 66% of the base material strength.

Microstructure analysis

Microstructures of samples loaded with a thermal cycle with increasing maximum temperatures have similar characteristics to the HAZ microstructure in real-life welds. The HAZ microstructure of investigated steel real-life welds has been evaluated in previous works [13, 17]. This means that the simulation of individual sub-zones is satisfactory. However, in contrast to the evaluation of the welded joint, this approach enables the evaluation of individual parts separately, thus supplementing the information regarding previous experiments. The microstructure of the base material without thermal loading is shown in Fig. 6(a). The microstructures of samples T550, T600, and T650 (shown in Figs. 6(b), (c), and (d), respectively) were typical of the SCHAZ sub-zone. This sub-critical zone, also called the "annealed zone", is the area where the temperature peaked below approximately 700°C. In this region, the A_{c1} temperature is not exceeded and, therefore, austenite is not formed. However, carbides may have been formed. The microstructures exhibit an almost complete martensitic microstructure with a very fine packet-size grain. The T800 sample microstructure shown in Fig. 6(e) is interesting, due to its inter-critical sub-zone. ICHAZ refers to HAZ regions which have been subjected to peak temperatures ranging between the upper and lower A_{c3} and A_{c1} critical points. The authors in [18] stated these temperatures to be in the range of 700-910°C. Temperatures of phase transformations of the studied steel S960MC

TABLE 3

Results of the tensile test for the base material (BM) and experimental samples

Sample No.	Average value of $R_{p0.2}$ [MPa]	Average value of R_m [MPa]	$R_{p0.2}$ / R_m	Sample No.	Average value of $R_{p0.2}$ [MPa]	Average value of R_m [MPa]	$R_{p0.2}$ / R_m
BM	1007.0	1092.0	0.92	T800	643.0	830.0	0.77
T550	950.5	960.5	0.99	T1000	803.5	920.0	0.87
T600	886.8	905.0	0.98	T1200	690.0	808.5	0.85
T650	822.5	840.0	0.98	T1350	649.0	727.0	0.89

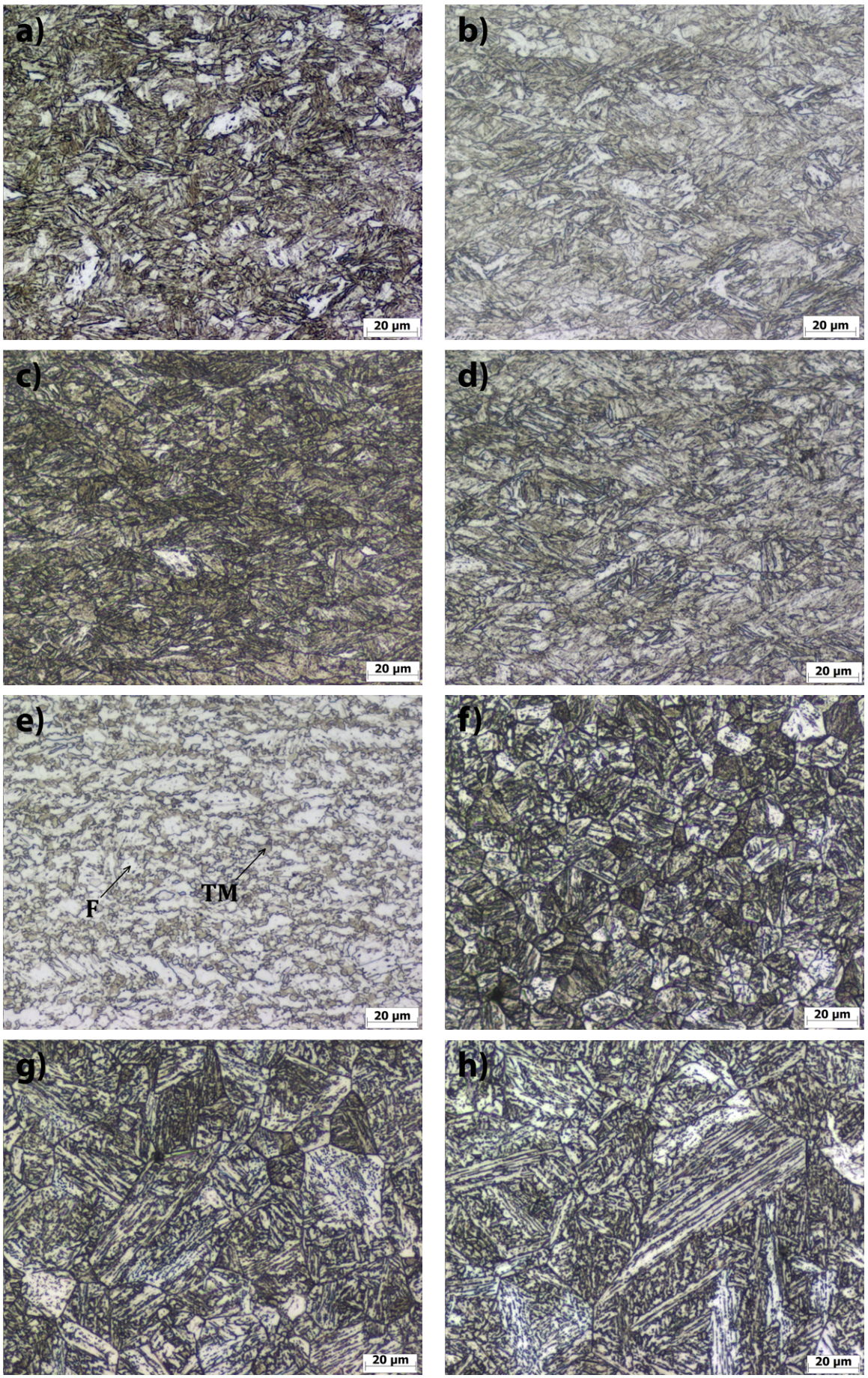

Fig. 6. Microstructure in the sample centre: (a) BM; (b) T550; (c) T600; (d) T650; (e) T800, F – ferrite, TM – tempered martensite; (f) T1000; (g) T1200; (h) T1350

by dilatometric tests were determined; namely, $Ac_3 = 870°C$ and $Ac_1 = 773°C$. In this region, partial re-transformation to austenite occurs during heating, the exact extent of which is governed by the peak temperature within the intercritical temperature range. During cooling, the austenite regions decompose, to different extents and to various transformation products. The microstructure in this region consists of a mixture of bainite, tempered martensite, and ferrite. The microstructure of sample T1000, as shown in Fig. 6(f), is typical of a fine-grained sub-zone occurring during welding at temperatures between 900°C and 1100°C. Exposure to heat in this zone causes transformation of the base metal to austenite. However, due to the low temperature and very short duration of exposure followed by rapid cooling, the microstructure transforms to either one or a combination of martensite and/or bainite. These microstructural phases cannot be identified by light metallography. Due to the fine-grained structure, the sample achieves better mechanical properties, compared to the ICHAZ and CGHAZ sub-zones. The microstructures of samples T1200 and T1350 were typical of the CGHAZ sub-zone, the area closest to the weld metal. The temperature in this area can reach up to 1500°C during welding. The CGHAZ is the area which was heated high above the Ac_3 temperature. This leads to the transformation of the base material into austenite and grain growth. Following rapid cooling, the enlarged austenitic grains are transformed back into martensite. The amount of the austenite phase growth increases when getting closer to the fusion zone, which corresponds to the temperature increase in the same direction. Therefore, the T1350 sample microstructure shown in Fig. 6(h) has a larger grain size than the T1200 sample microstructure shown in Fig. 6(g). Both microstructures are formed of tempered and untempered martensite.

Charpy pendulum impact test and fracture surfaces

The results of the test measurements are shown in Fig. 7. The absorbed energy values in all simulated samples were higher than those of the base material. With the exception of the value for T800 samples, the average absorbed energy increased with increasing maximum cycle temperature. For the T800 sample, the value of average absorbed energy was approximately the same as for the base material.

Observation of the fracture surface topography of the broken samples after the Charpy impact tests using scanning electron microscopy (SEM) only revealed ductile fractures. Microscopically, we observed pure transcrystalline ductile fractures with typical dimple morphology, without any signatures of intercrystalline or brittle fractures. Variations in the dimple size were affected by the HAZ microstructural features. The fracture surfaces of samples T550, T600, and T650 shown in Figs. 8(a), (b), and (c), respectively, which contained small and large dimples. Small dimples are related to the fine-grained microstructure of these samples. Large dimples are formed around large Fe_3C carbide particles, which are reduced at higher temperatures due to the partial dissolution of these carbides. The fracture surface of the T800 sample, as shown in Fig. 8(d), contained only small ductile dimples. The sizes of the dimples were related to the microstructure grain size. The fracture surfaces of samples T1000, T1200, and T1350, as shown in Figs. 8(e), (f), and (g), respectively, contained larger ductile dimples than the previous samples. Although the fracture surfaces had large ductile dimples, only relatively small carbide particles were present at their bottoms. These carbide particles were much smaller than the carbide particles at the bottoms of the large ductile dimples found on samples T550, T600, and T650.

Hardness tests

The average microhardness values of the base material and samples affected by the thermal cycle with different maximum cycle temperature are presented in Table 4 and graphically shown in Fig. 9.

Microhardness decreased with increasing maximum temperature of the thermal cycle. This decrease is related to the

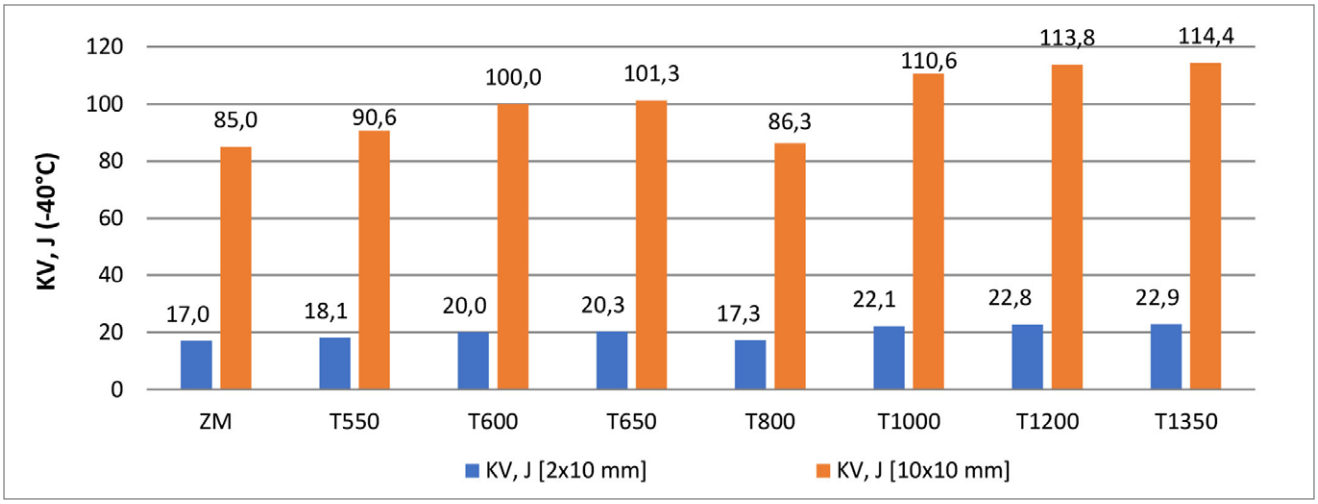

Fig. 7. Absorbed energy for base material and samples affected by the different maximum temperature

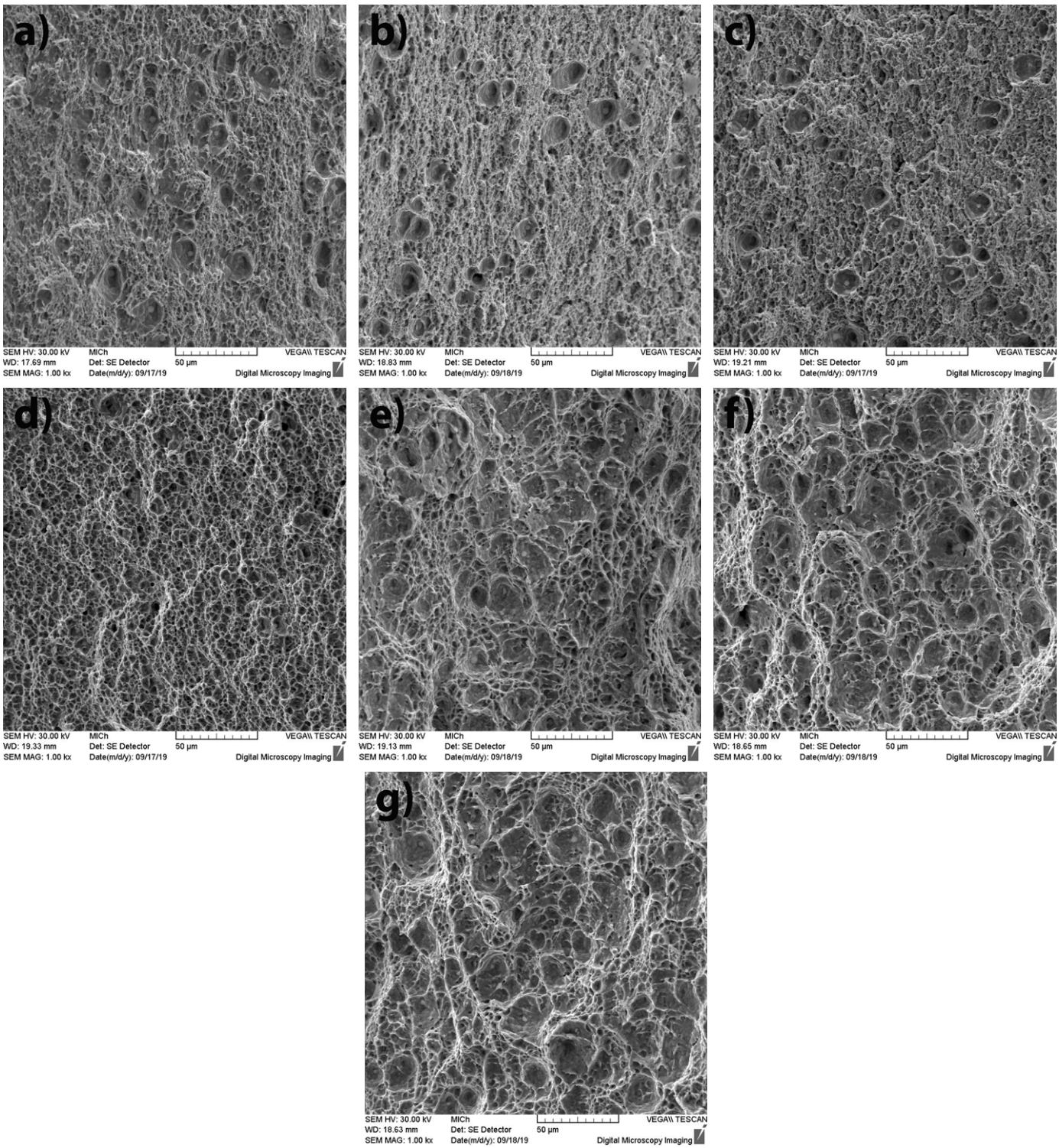

Fig. 8. SEM micrographs of the fracture surface after Charpy pendulum impact test with different maximum temperature: (a) T550; (b) T600; (c) T650; (d) T800; (e) T1000; (f) T1200; (g) T1350

TABLE 4

Results of the hardness test for the base material (BM) and experimental samples

Sample No.	HV1	Sample No.	HV1
BM	361	T800	251
T550	320	T1000	292
T600	285	T1200	260
T650	287	T1350	248

tempering of martensite in the base metal structure. The largest decrease was observed at a temperature of 800°C (251 HV1). In the T1000 sample, the microhardness increased again and reached a value of approx. 292 HV1. This is due to the favourable fine-grained structure of the FGHAZ zone. The hardness of the samples decreased again at higher maximum temperatures of the thermal cycle. The lowest values of microhardness were obtained in samples T1350 and T800, where only 69% of the

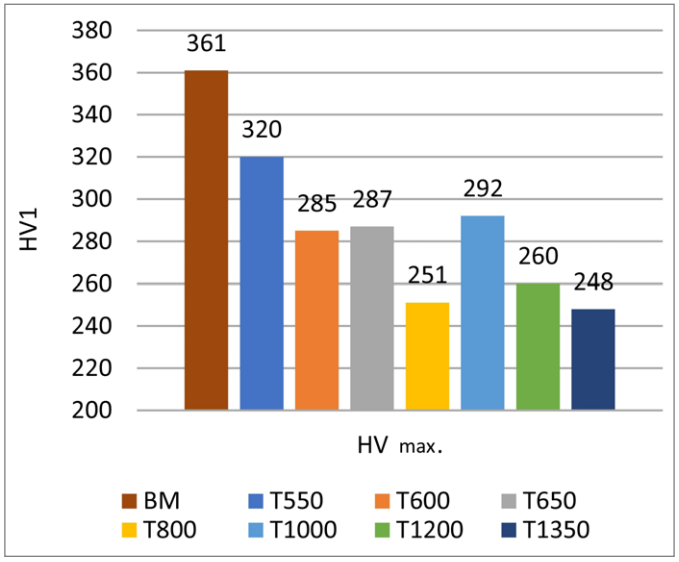

Fig. 9. Microhardness values of the base material and samples affected by the thermal cycle with different maximum cycle temperature

base metal hardness was recorded. This decrease in hardness corresponds to changes in strength. Decrease of strength-related properties is a typical behaviour for all high-strength steels (i.e., quenched, tempered, and TMCP steels), when they are heated in the range of 450°C to A_{c1} temperature, due to martensite tempering [23].

4. Conclusion

Physical simulation using the Gleeble device allowed samples to be exposed to the required temperature cycle. As a result, it was possible to create specific microstructures on samples corresponding to individual HAZ sub-zones, which further mechanical tests could be performed on. A summary of the values of all tested mechanical properties is shown graphically in Fig. 10.

The following conclusions can be drawn, based on this graph and the experimental results:

- Thermal loading of samples with a thermal cycle with different maximum temperatures caused the formation of a microstructure similar to the HAZ subzone of a real weld joint. Samples T550, T600, and T650 corresponded to the microstructures of the SCHAZ region; sample T800 had the characteristics of an ICHAZ zone; sample T1000 had the characteristics of an FGHAZ zone; and samples T1200 and T1350 corresponded in structure to the CGHAZ region.
- The T1350 samples achieved a tensile strength value by 33% lower than the base material. Samples T800 and T1350 had the most significant decrease in yield strength, where the value reached only 64% of that in the basic material. The authors of [5, 24] reached similar conclusions, but with other types of HSLA steels.
- There was no decrease in the value of absorbed energy in the individual sub-zones during the Charpy pendulum test.
- The CGHAZ zone is most often considered to be the most critical region, in terms of toughness. However, the absorbed energy in samples T1200 and T1350 increased by 34%, compared to the base material.
- Fracture surfaces in all tested samples (including the base material) had the same characteristics of transcrystalline ductile fractures with typical dimple morphologies.
- Variations in the dimple size were affected by the microstructural features of the HAZ and by the grain size.
- Changes in microhardness corresponded to the changes in tensile strength. The lowest values of microhardness were obtained in samples T1350 and T800, in which only 69% of the base metal hardness was recorded.
- The ICHAZ and CGHAZ zones are the most critical regions, in terms of mechanical properties. This phenomenon has also been noted in the works [5,6,25, 26], although the authors used other welding technologies and thicker steel sheets in these studies.

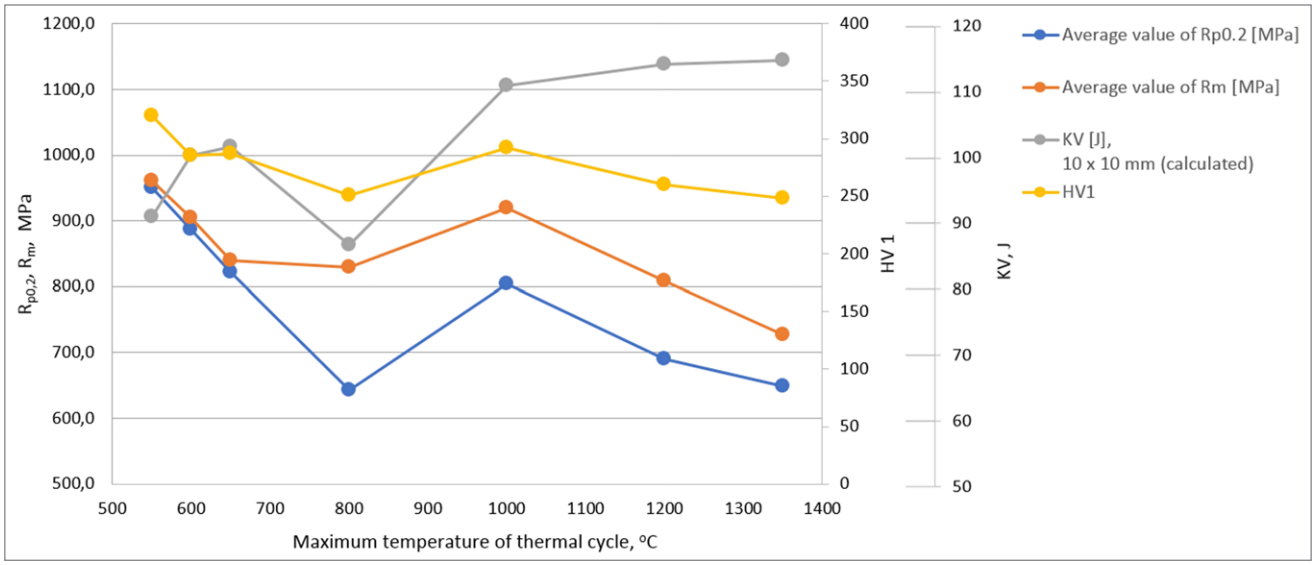

Fig. 10. Graphical representation of the results of all tested mechanical properties depending on the maximum value of the temperature cycle

The authors who published in the journal AMM focused on the welding of high-strength steels mainly by methods with highly concentrated heat sources. As in our study, changes in the microstructure in HAZ welded joints were significantly dependent on heat input and cooling rate. Lisiecki et al. [4], Błacha [12], Kurc-Lisiecka [24], and Górka [25,28,29] also found a heterogeneous microstructure composed of several subzones in the HAZ. Regardless of the type of HSLA steel, they described a coarse-grained structure (CGHAZ) located near the fusion line. Of interest was a significant decrease in toughness in this zone of Strenx 1110MC steel, up to 60% of that in the base material, as reported in [24]. This trend was contrary to the one observed in our study, where toughness increased in this zone. The decrease in hardness in two zones – CGHAZ and ICHAZ – was comparable to other studies, where the value of this decrease is determined by the type of steel. An interesting finding is the results in [12]: In a tensile test of S960QL laser-welded joints, the tensile strength values were above the required value for the given steel. For both S960QL and S960MC steels, the required strength range was almost the same (980-1250 MPa). Beam technologies are also suitable for the steel considered here, and further research will therefore be focused on this area.

Acknowledgement

This research was funded by APVV, grant number APVV-16-0276; KEGA, grant number KEGA 009ŽU-4/2019; and VEGA, grant number VEGA 1/0951/17. The authors hereby thank these agencies for their support.

REFERENCES

[1] C. Schneider, W. Ernst, R. Schnitzer, H. Staufer, R. Vallant, N. Enzinger, Welding in the World **62**, 801-809 (2018), DOI:10.1007/s40194-018-0570-1.

[2] R. Branco, F. Berto, Metals **8**, 610, (2018), DOI:10.3390/met8080610.

[3] M. Klein, H. Spindler, A. Luger, R. Rauch, P. Stiaszny, M. Eigelsberger, Materials Science Forum 500-501, 543-550 (2005), DOI: 10.4028/www.scientific.net/msf.500-501.543.

[4] A. Lisiecki, Archives of Metallurgy and Materials **61** (1), 93-102, (2016), DOI: 10.1515/amm-2016-0019.

[5] F. Hochhauser, W. Ernst, R. Rauch, et al., Weld World **56**, 77-85 (2012), DOI: 10.1007/BF03321352.

[6] J. Nowacki, A. Sajek, P. Matkowski, Archives of Civil and Mechanical Engineering **16** (4), 777-783, 2016, DOI: 10.1016/j.acme.2016.05.001.

[7] X.Z. Chen, Y.M. Huang, Z. Shen, J. Chen, Y.C. Lei, J.Z. Zhou, Science and Technology of Welding and Joining **18** (4), 272-278 (2013), DOI: 10.1179/1362171812Y.0000000095.

[8] J. Lago, L. Trško, M. Jambor, F. Nový, O. Bokůvka, M. Mičian, F. Pastorek, Metals **9** (6), 619 (2019), DOI: 10.3390/met9060619.

[9] M. Blatnický, M. Sága, J. Dižo, M. Bruna, Materials **13** (4), 817 (2020), DOI: 10.3390/ma13040817.

[10] W. Guo, L. Li, S. Dong, D. Crowther, A. Thompson, Optics and Lasers in Engineering **91**, 1-15, (2017), DOI: 10.1016/j.optlaseng.2016.11.011.

[11] P. Kopas, M. Sága, M. Jambor, F. Nový, L. Trško, L. Jakubovičová, MATEC Web of Conferences **244**, 01009, (2018), DOI: 10.1051/matecconf/201824401009.

[12] S. Błacha, M.S. Węglowski, S. Dymek, M. Kopyściański, Archives of Metallurgy and Materials **62** (2), 627-634 (2017), DOI: 10.1515/amm-2017-0092.

[13] M. Mičian, D. Harmaniak, F. Nový, J. Winczek, J. Moravec, L. Trško, Metals **10** (2), 229, (2020), DOI:10.3390/met10020229.

[14] T. Mohandas, G.M. Reddy, B.S. Kumar, Journal of Materials Processing Technology **88** (1-3), 284-294 (1999), DOI: 10.1016%2Fs0924-0136%2898%2900404-x.

[15] J. Laitila, J. Larkiola, Weld World **63**, 637-646 (2019). DOI: 10.1007/s40194-018-00689-7.

[16] Y. Shi, K. Sun, S. Cui, M. Zeng, J. Yi, X. Shen, Y. Yi, Materials **11**, 167 (2018), DOI: 10.3390/ma11010167.

[17] M. Jambor, R. Ulewicz, F. Nový, O. Bokůvka, L. Trško, M. Mičian, D. Harmaniak, Materials Research Proceedings **5**, 78-83 (2018) DOI: 10.21741/9781945291814-14.

[18] D. Stemne, T. Narström, B. Hrnjez, Welding Handbook. A guide to better welding of Hardox and Weldox, Edition 1, SSAB Oxelösund AB. ISBN 978-91-978573-0-7.

[19] Y. Guo, L. Lin, D. Zhang, L. Liu, M. Lei, Metals **8**, 773 (2018), DOI: 10.3390/met8100773.

[20] R. Pastircak, J. Scury, Archives of Metallurgy and Materials **62** (4), 2193-2198 (2017), DOI: 10.1515/amm-2017-0323.

[21] M. Bruna, L. Kucharcik, Materiali in Tehnologije **48** (6), 949-952 (2014).

[22] W. Guo, D. Crowther, J.A. Francis, A. Thompson, Z. Liuc, L. Li, Materials and Design **85** (15), 534-548 (2015), DOI: 10.1016/j.matdes.2015.07.037.

[23] V. Lazic, Metalurgija **55** (2), 213-216 (2016), https://hrcak.srce.hr/146500.

[24] A. Kurc-Lisiecka, J. Piwnik, A. Lisiecki, Archives of Metallurgy and Materials **62** (3), 1651-1657 (2017), DOI: 10.1515/amm-2017-0253.

[25] J. Górka, Archives of Metallurgy and Materials **60** (1), 469-475 (2015), DOI: 10.1515/amm-2015-0076.

[26] H. Ismar, Z. Burzic, N.J. Kapor, T. Kokelj, Strojniški vestnik – Journal of Mechanical Engineering **58** 6, 422-428 (2012), DOI:10.5545/sv-jme.2011.281.

[27] S. Ślęzaka, L. Śnieżeka, Procedia Engineering **114**, 78-85 (2015), DOI: 10.1016/j.proeng.2015.08.044.

[28] J. Górka, Metals **8**, 169 (2018); DOI:10.3390/met8030169.

[29] J. Górka, A. Kotarska, IOP Conference Series: Materials Science and Engineering **591**, 012017, 1-8 (2019).